IEEE Access
Multidisciplinary | Rapid Review | Open Access Journal

Received February 22, 2021, accepted March 8, 2021, date of publication March 12, 2021, date of current version March 23, 2021.

Digital Object Identifier 10.1109/ACCESS.2021.3065729

Synthesis and Design of Highly Selective Multi-Mode Dual-Band Bandstop Filter

MUHAMMAD FAISAL, SOHAIL KHALID, (Member, IEEE), MUJEEB UR REHMAN, AND MUHAMMAD ABDUL REHMAN

Department of Electrical Engineering, Riphah International University, Islamabad 44000, Pakistan

Corresponding author: Muhammad Faisal (muhammad.faisal@riphah.edu.pk)

ABSTRACT This paper presents the synthesis and design of the multi-mode dual-band bandstop filter (MM-DBBSF). A highly selective multi-mode dual-band bandstop response is obtained using a quarter wavelength coupled line structure. It has been shown that by increasing the coupled line's order, the selectivity and the transmission zeros are increased in the desired stopband. Moreover, a step impedance resonator (SIR) is used between two coupled lines to achieve more transmission poles for better out of band selectivity. The paper show a detailed theoretical synthesis of the coupled line and SIR structure. In order to validate the theoretical model, ideal and microstrip topologies are designed and simulated. Furthermore, a high-frequency substrate is used to fabricate four prototypes. The simulated and measured results show good concurrence.

INDEX TERMS Bandstop filter, microstrip filter, coupled line, step impedance resonator.

I. INTRODUCTION

Noise is a big concern while designing modern closely sited wireless communication systems that are operable at microwave frequencies. Bandstop filters (BSFs) play an essential role in mitigating the unwanted noise signals within the desired band. Different design topologies have been adopted in the previous years to overcome the problem of unwanted signals.

In [1], the BSF has been designed using the SIR technique. The author managed to produce a narrow and wideband bandstop response by incorporating the SIR and spur line. However, the frequency response shows poor out of band rejection. Moreover, the selectivity on the lower frequency side is also poor.

The coupled line connected in parallel with the transmission line technique has been observed in [2] to achieve BSF. Sharp wideband rejection having four transmission zeros in the stopband is obtained; however, this topology provides low rejection levels at the upper passband and increased fabricated prototype size.

A wideband BSF filter was realized using the coupled line section [3]. The location of the transmission zeros and rejection level is controlled by varying the coupled line's length. However, the measured result shows few discrepancies with the simulated results due to microstrip bends and discontinuities.

In recent years, the demand for multiband wireless communication systems has been increased significantly. Therefore, many techniques are presented to achieve the multiband bandstop frequency response [4]–[23]. The stepped impedance resonator technique was integrated to realize dual-band bandstop filters (DBBSFs) response [4]–[11]. The filter design in [4] uses a single SIR that mainly focuses on the size reduction of the filter; the measured results display that the out of band insertion is very poor. However, it is challenging to design a more compact size DBBSF; an extension to [4], a tri-section stepped impedance resonator (TSSIR) was realized to accommodate the size issues [5]. The measured result shows very high insertion loss in the upper passband from 6 GHz to 8 GHz, and also, the out of band selectivity is not improved to the mark. A modified version of SIR known as Hairpin structures is popular in designing low pass filters [6], [7], whereas, in [8], hairpin structure is embedded with two open stubs was implemented to acquire DBBSF response. The result shows the two TZs at each stopband, and the overall measured response is very poor. However, in [9], the same hairpin structure has been used with a good stopband response. The filter order has been increased by implementing an identical hairpin over the same transmission line, which gives a good rejection level better than 20dB for both stopbands, but the

The associate editor coordinating the review of this manuscript and approving it for publication was Shaoyong Zheng.

insertion loss in the upper passband is a bit high. Moreover, the modified SIR structures that include circular, folded, symmetric-type, meandered lines have been incorporated to achieve the DBBSF filter. These structural modifications are used to achieve miniaturization, and better out of band selectivity [10]. Wideband DBBSF response has been observed using the second-order stub enclosed SIR (SE-SIR) structure [11]. The selectivity of the filter is enhanced because of two TZs in each stopband. By incorporating the enclosed stub to the conventional SIR, the structure can generate wide stopbands in the very close region. However, the out of band selectivity is very poor, and the insertion loss at the upper passband is very high.

The coupled line technique has been investigated in [12]–[15] to accomplish the DBBSF filter response. Selectivity and better rejection have been obtained by integrating the coupled line section's technique, and cross-coupled capacitor in a dual-mode loop resonator [12]. The DBBSF response gives more than 20dB rejection at the stopbands, but the upper passband insertion loss is high. In [13], second-order and third-order wideband DBBSF has been presented. Both second-order and third-order filters have two paths; for the second-order filter, path 1 has a stub loaded transmission line, and path 2 has open-ended coupled lines. In comparison, the third-order filter is incorporated with a T shape structure in path 2. It has been observed that the bandwidth and the selectivity has been refined for the third-order DBBSF filter as compared to the second-order DBBSF filter. Characteristic impedance and the coupling coefficient of the two transmission paths can also tune the isolation of stop bands independently. A new coupled line structure technique has been analyzed to attain the DBBSF filter [14]. Two symmetrical coupled lines have been used to obtain dual-band bandstop features. Moreover, the size of the fabricated work is reduced through the coupling of transmission lines. The result shows high skirt selectivity and sharp rejection. In [15], Zhang *et al.* presented a coupling technique of stepped impedance resonator. Extended bandwidth of the stopbands and high selectivity has been acquired through coupling; out of band selectivity is good for the lower passband, but the upper passband's selectivity from 5 GHz to 6 GHz is compromised.

Moreover, the topologies of the triple band bandstop filter (TBBSF) is also presented in [16]–[20]. Trisection meandered line open-end SIR has been used to realize triple-band response [16]. The design has been analyzed for symmetrical and asymmetrical SIR over the transmission line; moreover, bending has been incorporated to achieve further size reduction. The measured result shows good concurrence with the simulated results, displaying high rejection at three stopbands, but the insertion loss throughout the frequency sweep is not good. Min *et al.* presented a TBBSF using a folded square stepped impedance resonator technique [17]. Defected microstrip structure (DMS) is coupled with SIR cells to achieve three-stop bands with enhanced rejection level. Owing to the SIR cells can reduce the total size of the structure. The measured result displays the compromised out of band selectivity and very high insertion loss. Coupled line stub loaded shorted SIR (CLSLSIR) has been presented in [18] to realize the TBBSF response; however, the measured result has a lot of distortion in the lower and upper passbands, and also the rejection level of the first stopband is not promising. First and second-order TBBSF filter has been designed using the stub loaded SIR technique [19]. The second-order filter has been fabricated and measured that shows promising rejection levels of the stopbands, whereas selectivity of the passbands is very poor. To realize the TBBSF response, a cross-shaped microstrip resonator is proposed and designed; however, the insertion loss is very high in all the passband regions [20]. The integration of SIR with different formation has been proposed in [21]–[23] to achieve quad-band bandstop filter (QBBSF) response.

In this paper, an MM-DBBSF topology is proposed based on coupled line and SIR structure. The designed topology produces a multiband bandstop response with high rejection at the stop bands, and good out of band selectivity. The detailed synthesis of the coupled line structure has been presented. It has been analyzed that the parameter variations in a coupled line structure gives better selectivity and produce a multimode response. Moreover, the harmonic suppression and enhanced out of band selectivity can be controlled by integrating the SIR structure. Four different microstrip prototypes are fabricated on a high-frequency substrate and measured using Agilent N5242A PNA-X to validate the proposed topology.

II. DESIGN METHODOLOGY

Fig. 1 shows the MM-DBBSF topology. The topology consists of the N_{th} order quarter wavelength couple line structure separated by a wavelength long N_{th} order SIR structure. The single unit cell produces a dual-band response. The SIR structure behaves like a low pass filter, which suppresses the harmonics and enhances out of band selectivity.

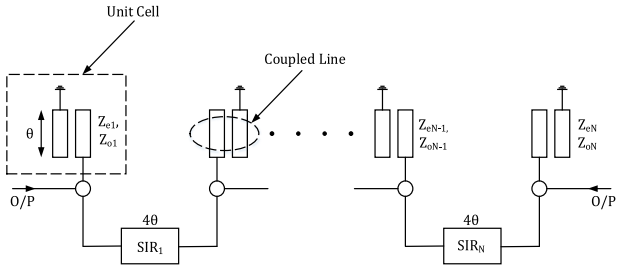

FIGURE 1. Multimode dual-band bandstop filter (MM-DBBSF) topology.

A. PROPOSED COUPLED LINE STRUCTURE

Fig. 2 displays the coupled line structure's equivalent circuit model. The equivalent circuit comprises an open and short-circuited stub. The impedance of open-circuited stub is Z_{oc}, whereas the impedance of short-circuited stub is Z_{sc}.

The evaluated impedance values are given in (1) and (2).

$$Z_{oc} = \frac{2\,Z_e Z_o}{(Z_e + Z_o)} \tag{1}$$

$$Z_{sc} = \frac{(Z_e - Z_o)^2}{2\,(Z_e + Z_o)} \tag{2}$$

The synthesis of the coupled line structure is presented to validate the proposed equivalent circuit. The transfer matrix of the coupled line structure is extracted using the distributed equivalent circuit model. By using the transmission coefficient formula given in [24] the filtering function is calculated as:

$$F_N = \frac{1}{2}\left(\frac{(Z_{oc} + Z_{sc})\,cos^2\theta - Z_{oc}}{cos\theta\ sin\theta}\right) \tag{3}$$

The filtering function is 2_{nd} order and can be easily mapped to the Chebyshev type-I filtering response. However, there is a frequency-dependent term in the denominator that will alter the frequency response. The second-order Chebyshev type-I is of form $F_N = Acos^2\theta - B$. Furthermore, it has been investigated that increasing the values of the coefficients A and B of the general form with the ratio 2:1 will approximate the actual frequency response of the coupled line structure. As evident from the filtering function, the single coupled line structure shown in Fig. 2 gives the dual-band bandstop notches; however, based on the analysis, it has been observed that by increasing the order of the coupled line structure having the same impedance and electrical length values will produce a more selective response.

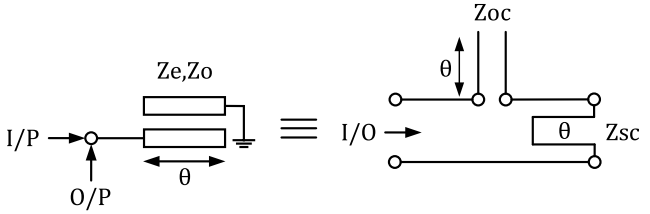

FIGURE 2. Equivalent circuit of coupled line structure.

To provide the evidence Fig. 3 shows the response of up to fourth-order coupled line structure having the constant values of $Z_e = 219\ \Omega$, $Z_o = 68\ \Omega$ and $\theta = 87.6$. The first order coupled line structure response clearly shows that the maximum rejection level is 30.59 dB, whereas the insertion loss is 9.89 dB at 1.35 GHz and 2.65 GHz frequencies. However, the second, third, and fourth-order coupled line structure gives the maximum rejection of 36.63 dB, 40.16 dB, and 42.66 dB, respectively, whereas the insertion loss is 15.29 dB, 18.64 dB, and 21.07 dB for the second, third, and fourth-order at 1.35 GHz and 2.65 GHz frequencies, respectively. It can be seen that selectively is increasing as the order of the coupled line structure is increasing.

Moreover, the center frequency of the transmission zeros can be adjusted through the variation of the coupling coefficient (Z_e, Z_o, θ). This variation can be observed in Fig. 4.

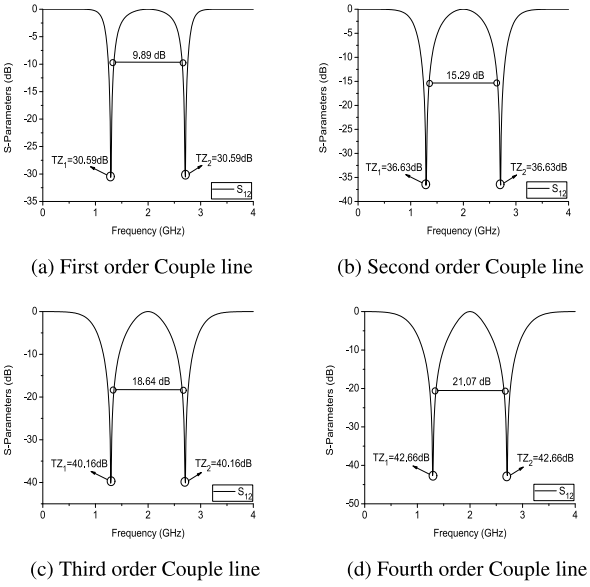

(a) First order Couple line (b) Second order Couple line

(c) Third order Couple line (d) Fourth order Couple line

FIGURE 3. Comparison of responses up to fourth order coupled line structure.

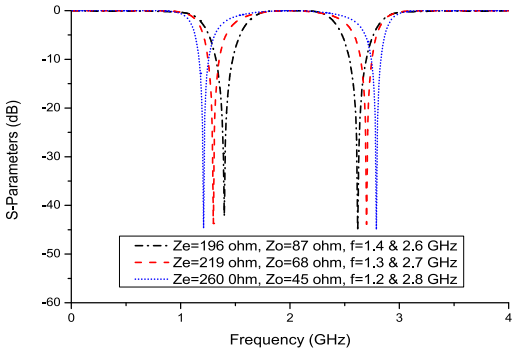

FIGURE 4. Resonate frequency tuning by varying coupling coefficients.

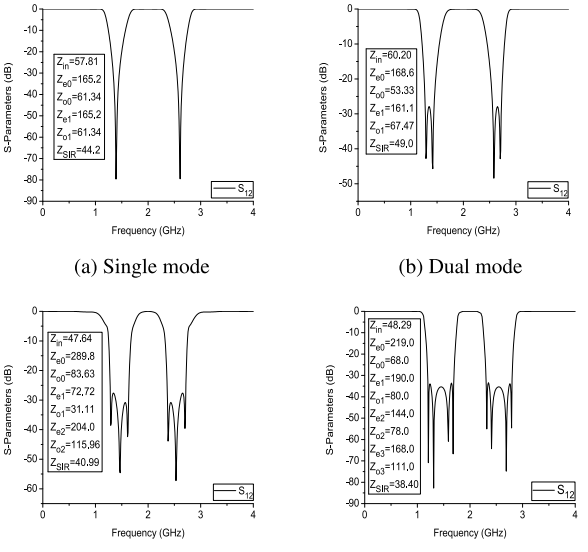

(a) Single mode (b) Dual mode

(c) Triple mode (d) Quad mode

FIGURE 5. Coupled line structure having different even-odd impedances with constant electrical length.

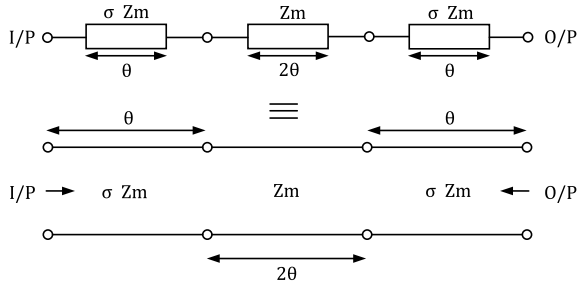

FIGURE 6. SIR structure.

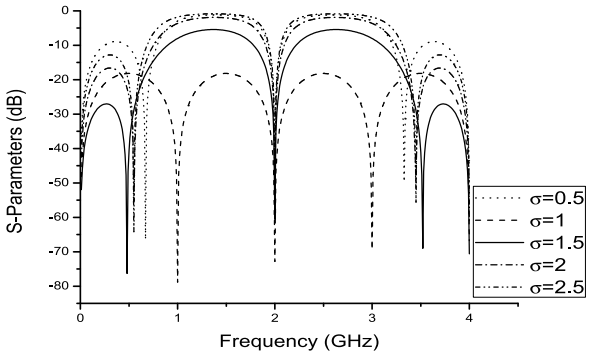

FIGURE 7. Comparison of S_{11} for different values of impedances.

It can be seen that by increasing the value of Z_e, the first transmission zero will move towards the lower frequency, whereas the second transmission zero moves towards the higher frequency and vice versa. Moreover, by increasing the value of Z_o, the first transmission zero moves towards the higher frequency, whereas the second transmission zero moves towards the lower frequency and vice versa.

Furthermore, it has also been observed that increasing the order of the coupled line structure with different values of impedances will produce a multi-mode response.

Fig. 5 displays the graphs of coupled line structure for N = 1 to 4. It can be observed that by increasing the order of coupled line structure with different impedance values, the in-band transmission zeros are increased, hence provide a multi-mode response. With this mode increment, the bandwidth and the selectivity of the bandstop filter are improved. The impedance values are also listed in the Fig. 5.

B. SIR STRUCTURE

The full wavelength SIR structure shown in Fig. 6 is incorporated to suppress the harmonics and improved the out of band selectivity. The SIR structure consists of two quarter wavelength transmission lines with the characteristic impedance of σZ_m separated by a half wavelength transmission line of impedance Z_m.

Frequency response S_{11} for different values of σ is plotted in Fig. 7. It is required to obtain suppression below 0.5 GHz and above 3.5 GHz while maintaining a better in-band return loss level. Ideally, when $\sigma = 1.5$, the best-desired response is achieved. However, due to the effects of microstrip losses, the σ value is slightly optimized to 1.7.

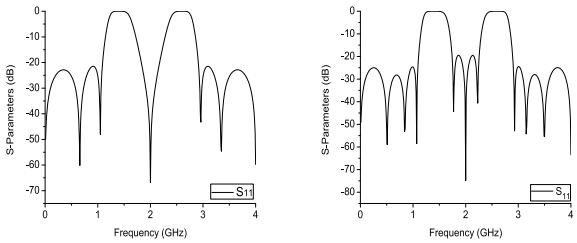

(a) First order SIR (b) Second order SIR

FIGURE 8. Comparison of first and second order SIR.

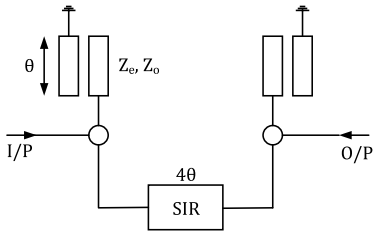

FIGURE 9. Topology of the proposed structure.

The transfer matrix of SIR structure is calculated using (6). The calculated filtering function in (7) is of Chebyshev type-I with a frequency-dependent term in numerator. The effect of this term is compensated in the filtering coefficients by using the synthesis procedure opted in [25].

$$[T]_1 = \begin{bmatrix} cos\theta & j\sigma Z_m sin\theta \\ \dfrac{jsin\theta}{\sigma Z_m} & cos\theta \end{bmatrix} \tag{4}$$

$$[T]_2 = \begin{bmatrix} cos2\theta & jZ_m sin2\theta \\ \dfrac{jsin2\theta}{Z_m} & cos2\theta \end{bmatrix} \tag{5}$$

$$[T]_{SIR} = [T]_1 \times [T]_2 \times [T]_1 \tag{6}$$

$$F_N = sin\theta \left(A\, cos^3\, \theta - Bcos\theta \right) \tag{7}$$

where;

$$A = \frac{(\sigma+1)(\sigma^3 Z_m^3 + \sigma^2 Z_m^2 - \sigma - 1)}{\sigma^2 Z_m}$$

$$B = \frac{(\sigma+1)(\sigma^3 Z_m^2 - 1)}{\sigma^2 Z_m}$$

Fig. 8 shows the effect of first and second-order SIR on the frequency response. The first order SIR introduce seven transmission poles, whereas second-order SIR produce eleven transmission poles. It can be seen that the second-order SIR provides better selectivity. However, the overall loss will be increased.

C. PROPOSED STRUCTURE

Fig. 9 shows the proposed structure with two identical couple lines separated by a SIR.

The coupled line structure is responsible for generating two transmission zeros at 1.4 GHz and 2.6 GHz. Whereas,

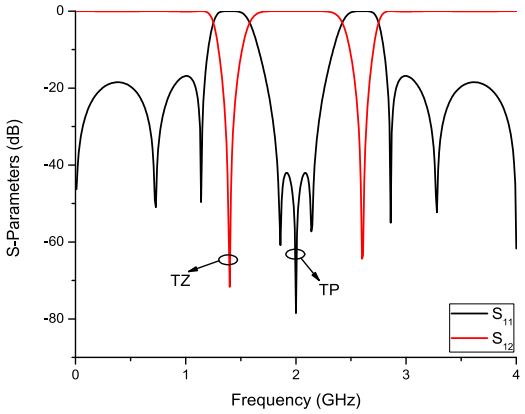

FIGURE 10. Response of proposed structure.

SIR integrated with couple line is responsible for generating nine transmission poles out of which seven are at the finite frequency, which will further enhance the selectivity and better out of band rejection as depicted in Fig. 10.

The filtering function of the proposed structure is calculated and given in (11).

$$[T]_{CL} = \begin{bmatrix} A & B \\ C & D \end{bmatrix} \tag{8}$$

$$[T]_{SIR} = \begin{bmatrix} A' & B' \\ C' & D' \end{bmatrix} \tag{9}$$

$$[T]_{Total} = [T]_{CL} \times [T]_{SIR} \times [T]_{CL} \tag{10}$$

$$F_N = \left(\frac{\alpha\, Cos^6\,\theta - \beta Cos^4\,\theta + \gamma Cos^2\,\theta - \zeta}{\sigma^4 Z_m^2 (\, Cos^4\,\theta - Cos^2\,\theta)} \right) \tag{11}$$

where;

$$\alpha = (\sigma+1)^2(Z_m\sigma + Z_{oc} + Z_{sc} + 1)(Z_m\sigma + Z_{oc} + Z_{sc} - 1)$$

$$\beta = 2(\sigma+1)(Z_m^2\sigma^3 + \frac{Z_m\sigma^2}{2}(Z_m + 2Z_{oc} + 4Z_{sc}) + \sigma(Z_{sc}^2 + (2Z_m + Z_{oc})\, Z_{sc} + Z_m Z_{oc} - \frac{1}{2} + \frac{1}{2}Z_{oc}^2 + 2Z_{sc}Z_{oc} + \frac{3}{2}Z_{sc}^2 - 1)$$

$$\gamma = Z_m^2\sigma^4 + Z_m\sigma^3\,(Z_m + 2Z_{sc}) + \sigma^2(Z_m Z_{oc} + 5Z_m Z_{sc} + Z_{sc}^2) + \sigma\left(-1 + 4Z_{sc}^2 + (2Z_m + 2Z_{oc})\, Z_{sc}\right) + 2Z_{sc}Z_{oc} + 3Z_{sc}^2 - 1$$

$$\zeta = Z_{sc}(Z_m\sigma^2 + Z_{sc}\sigma + Z_{sc})$$

The shown filtering function verifies the existence of two transmission zeros that can be seen from Fig. 5. Moreover, by using the unitary condition, the reflection coefficient is calculated in terms of filtering function. The resultant reflection coefficient will produce nine transmission poles, which is evident from Fig. 10.

III. FABRICATED PROTOTYPES

In order to validate the proposed topology, a total of four prototypes are fabricated on microstrip substrate Roger Duroid 5880. The ideal electrical parameters are converted to physical parameters using the line calculator. The effects of substrate loss are corrected using tuning and optimization in full EM simulations.

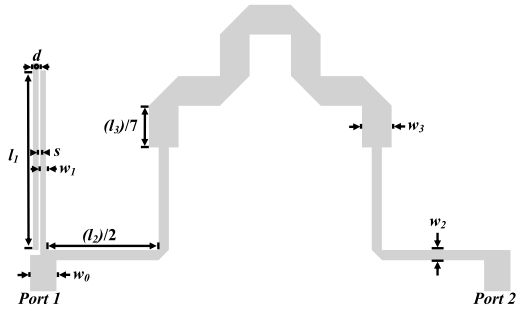

FIGURE 11. Top view of the prototype-1 ($l1 = 24.599$ mm, $l2 = 28.116$ mm, $l3 = 39.746$ mm, $w0 = 3.620$, $w1 = 0.8$ mm, $w2 = 1.411$ mm, $w3 = 4.084$ mm, $s = 0.2$ mm, $d = 0.4$ mm, $0.65\lambda_g \times 0.388\lambda_g$).

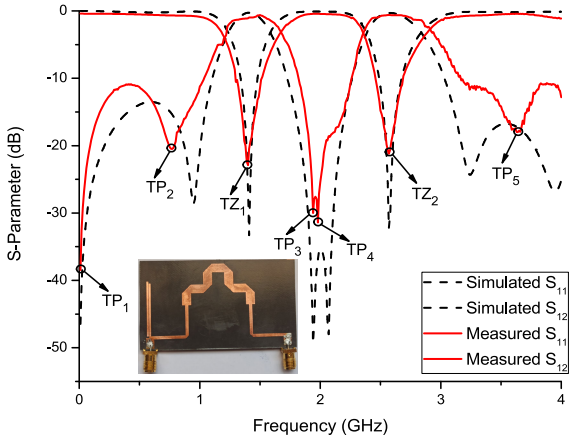

FIGURE 12. Simulated and measured results of fabricated prototype-1.

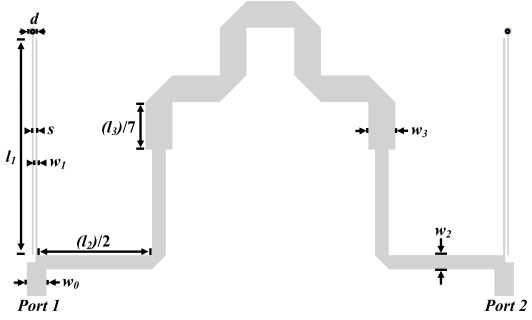

FIGURE 13. Top view of the prototype-2 ($l1 = 28.355$ mm, $l2 = 26.974$ mm, $l3 = 42.511$ mm, $w0 = 2.610$ mm, $w1 = 0.356$ mm, $w2 = 1.585$ mm, $w3 = 3.545$ mm, $s = 0.383$ mm, $d = 0.4$ mm, $0.617\lambda_g \times 0.37\lambda_g$).

The prototype-1 with the single coupled line integrated with SIR is fabricated to back up the theoretical analysis that single coupled line structure is solely responsible for generating two stopband notches as shown in Fig. 11. The input-output lines are extended for SMA soldering.

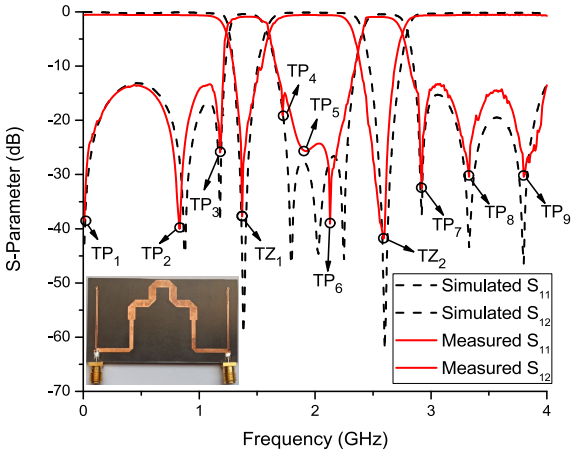

FIGURE 14. Simulated and measured results of the fabricated prototype-2.

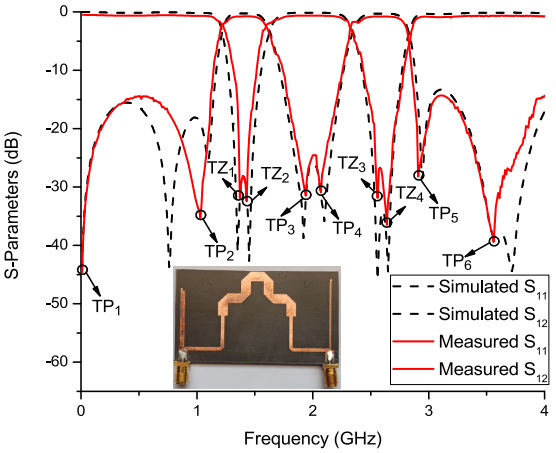

FIGURE 16. Simulated and measured results of the fabricated prototype-3.

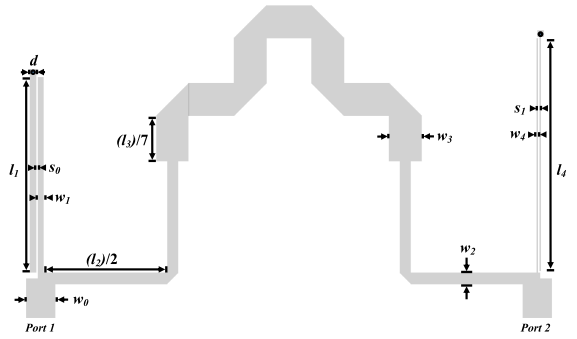

FIGURE 15. Top view of the prototype-3 ($l1 = 24.599$ mm, $l2 = 28.116$ mm, $l3 = 39.746$ mm, $l4 = 29.445$ mm $w0 = 3.620$ mm, $w1 = 0.8$ mm, $w2 = 1.411$ mm, $w3 = 4.084$ mm, $w4 = 0.201$ mm $s0 = 0.2$ mm, $s1 = 0.204$ mm, $d = 0.4$ mm, $0.65\lambda_g \times 0.388\lambda_g$).

Two stop bands at $f_1 = 1.40$ GHz and $f_2 = 2.57$ GHz are measured with the rejection level of 22.8 and 21.2 dB, respectively as shown in Fig. 12. Moreover, five transmission poles are measured at 0, 0.77, 1.94, 1.97, and 3.64 GHz. The mismatching of simulated and measured results is caused due to fabrication discrepancies, and parasitic behaviour of the SMA connector.

Prototype-2 consists of two coupled lines having the same physical parameters, and a single SIR integrated in between is fabricated, as shown in Fig. 13.

The two transmission zeros are measured to be at $f_1 = 1.37$ GHz and $f_2 = 2.59$ GHz, as shown in Fig. 14. The maximum rejection of 37.72 and 41.85 at the two stopbands are measured. Furthermore, nine transmission poles have been measured around the stop bands located at 0, 0.83, 1.74, 1.93, 2.13, 2.92, 3.33, and 3.80 GHz. Here, it is worth mentioning that the rejection level has been increased, and the selectivity around the stop bands has also been improved; moreover, the measured out of stop bands return loss is greater than 13 dB from 0 to 4 GHz as compared to the prototype-1 which was measured to be 10dB previously. The little disparity in simulated and measured results is due to the limitation of fabrication and errors in measurements. These discrepancies can be adjusted through the post-fabrication tuning.

To back up the analysis conducted in the above section of design methodology, the EM simulation and the fabrication has been done for the prototype-3, having different physical parameters of both the coupled lines integrated with the SIR in between as illustrated in Fig. 15.

It is evident that having different physical parameters of coupled line structure yields extra transmission zeros within the same stop band locality. Therefore, it is responsible for enhancing further stop band selectivity or adding modality in the response. Four transmission zeros are measured at 1.37, 1.43, 2.56, and 2.64 GHz having the rejection level of 31.86, 32.42, 31.87, and 36.47 dB, respectively, as shown in Fig. 16. The measured result displays a slight deviation from the simulated results because of unexpected tolerance in fabrication.

In addition to the fabrication of the prototype-3 having different physical parameters of coupled line structure, another fabrication of the prototype-4 having three coupled lines with different physical parameters and two SIR in between them has been done as shown in Fig. 17.

Here, it can be seen that the measured transmission zeros have been increased within the same stopband region, as shown in Fig. 18. Overall six transmission zeros are measured at 1.33, 1.41, 1.50, 2.55, 2.62, and 2.69 GHz having the rejection levels of 29.88, 33.90, 45.25, 41.49, 36.38 and 49.47 dB respectively. Similarly, a significant increase in transmission poles has also been measured as compared to the previous prototype 3. This is due to the addition of another SIR structure between the three coupled lines. Thirteen transmission poles are measured from 0 to 4 GHz which are located at 0, 0.43, 0.86, 1.07, 1.75, 1.97, 2.27, 2.41, 2.90, 3.15, 3.34, 3.57, and 3.83 GHz. Overall, 16 dB out of stopband return loss is achieved. The measured result shows good concurrence with the simulated results with a

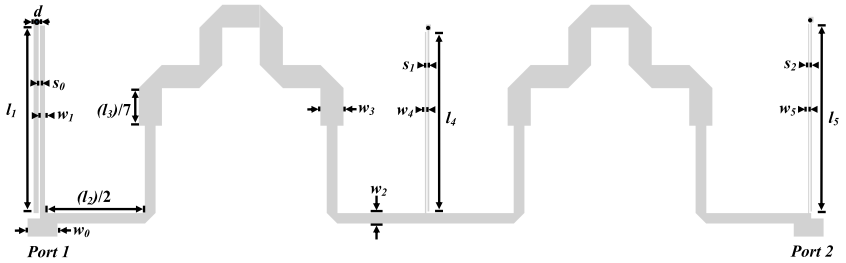

FIGURE 17. Top view of the prototype-4 ($l1 = 29.996$ mm, $l2 = 27.956$ mm, $l3 = 42$ mm, $l4 = 28.986$ mm, $l5 = 30.246$ mm, $w0 = 4.8$ mm, $w1 = 0.8$ mm, $w2 = 1.704$ mm, $w3 = 3.684$ mm, $w4 = 0.256$ mm $w5 = 0.2014$ mm, $s0 = 0.2028$ mm, $s1 = 0.2$ mm, $s2 = 0.2002$ mm, $d = 0.4$ mm, $1.26\lambda_g \times 0.367\lambda_g$).

TABLE 1. Comparison of the fabricated prototypes.

Fabricated Topology	Transmission zeros S_{12} 0-4 GHz	Transmission poles S_{11} 0-4 GHz	Out of stop band return loss (dB)	Maximum rejection level of stop band (dB)	Fractional band width of stop bands at 10dB(%)
Prototype 1	2	5	<-10	22.8	12.7, 10.11
Prototype 2	2	9	<-13	41.85	17.51, 12.74
Prototype 3	4	6	<-14	36.47	14.08, 13.02
Prototype 4	6	13	<-16	49.47	21.91, 13.2

TABLE 2. Comparison of measured results for some previously reported bandstop filters.

Reference Topologies	Transmission zeros S_{12}	Transmission poles S_{11}	Fractional band width at 10dB (%)	Frequencies (GHz)	Out of stop band return loss(dB)	Circuit size ($\lambda_g \times \lambda_g$)
[4]	2	5	56.7, 28.2	1.57, 3.16	<-8	0.44×0.37
[5]	2	6	40.4, 18	2.35, 5.58	<-10	1.09×0.70
[11]	4	3	31.02, 23.93	4.7, 6.64	<-10	0.51×0.09
[12]	4	3	100, 10	2.1, 6.4	<-15	0.48×0.55
[14]	2	5	22.6, 16.8	0.84, 1.13	<-10	0.22×0.49
This Work	2	5	12.7, 10.11	1.40, 2.57	<-10	0.65×0.38

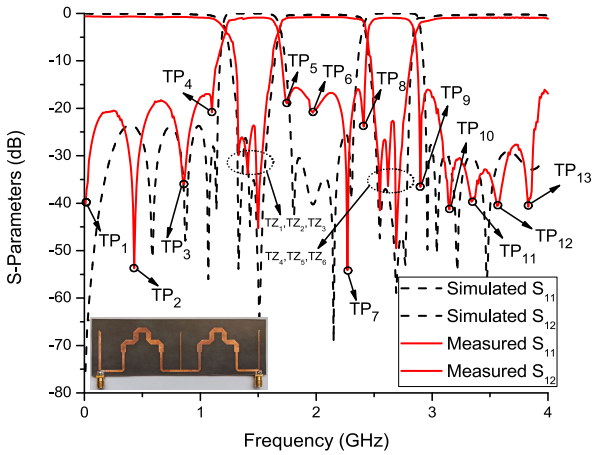

FIGURE 18. Simulated and measured results of the fabricated prototype-4.

slight frequency deviation. This deviation is due to the compromised fabrication precision and can be rectified through proper post-fabrication tuning.

Table 1 illustrates the measured results of all the fabricated prototypes.

Table 2 shows the comparison of the presented work with the previously reported work. The proposed work shows notable improvement in transmission poles and zeros. Moreover, a better return loss rejection level is attained.

IV. CONCLUSION

This paper presents the MM-DBBSF based on the coupled line and SIR structure. To verify the theoretical model, four prototypes have been fabricated on a high-frequency substrate and measured using Agilent N5242A PNA-X for the validation of the proposed topology. The measured results show good agreement with the theoretical and simulated work. Owing to its highly selective response and flexible design approach, the proposed MM-DBBSF is a good candidate for modern multi-band wireless systems to remove the unwanted signals.

REFERENCES

[1] Y.-Z. Wang and M.-L. Her, "Compact microstrip bandstop filters using stepped-impedance resonator (SIR) and spur-line sections," *IEE Proc. Microw., Antennas Propag.*, vol. 153, no. 5, p. 435, 2006.
[2] M. Á. Sanchez-Soriano, G. Torregrosa-Penalva, and E. Bronchalo, "Compact wideband bandstop filter with four transmission zeros," *IEEE Microw. Wireless Compon. Lett.*, vol. 20, no. 6, pp. 313–315, Jun. 2010.

[3] K. W. Qian and X. H. Tang, "Compact bandstop filter using coupled-line section," *Electron. Lett.*, vol. 47, no. 8, pp. 505–506, Apr. 2011.
[4] K.-S. Chin, J.-H. Yeh, and S.-H. Chao, "Compact dual-band bandstop filters using stepped-impedance resonators," *IEEE Microw. Wireless Compon. Lett.*, vol. 17, no. 12, pp. 849–851, Dec. 2007.
[5] C.-K. Lung, K.-S. Chin, and J. S. Fu, "Tri-section stepped-impedance resonators for design of dual-band bandstop filter," in *Proc. Eur. Microw. Conf. (EuMC)*, Oct. 2009, pp. 771–774.
[6] J.-H. Cho and J.-C. Lee, "Compact microstrip stepped-impedance hairpin resonator low-pass filter with aperture," *Microw. Opt. Technol. Lett.*, vol. 46, no. 6, pp. 517–520, Sep. 2005.
[7] J.-H. Cho and J.-C. Lee, "Microstrip stepped-impedance hairpin resonator low-pass filter with defected ground structure," *Microw. Opt. Technol. Lett.*, vol. 48, no. 2, pp. 405–408, Feb. 2006.
[8] S. Majidifar, S. V. A.-D. Makki, S. Alirezaee, and A. Ahmadi, "Dual-band bandstop filter using modified stepped-impedance hairpin resonators," in *Proc. 5th Int. Conf. Comput. Intell. Commun. Netw.*, Sep. 2013, pp. 61–63.
[9] J. Dzhumamuhambetov, A. Bakitgul, and A. Gorur, "A novel dual-band microstrip bandstop filter based on stepped impedance hairpin resonators," *Prog. Electromagn. Res. Lett.*, vol. 84, pp. 139–146, 2019.
[10] R. Dhakal and N.-Y. Kim, "A compact dual-band bandstop filter using a circular, folded, symmetric, meandered-line, stepped-impedance resonator," *Microw. Opt. Technol. Lett.*, vol. 56, no. 10, pp. 2298–2301, Oct. 2014.
[11] G. R. Koirala, B. Shrestha, and N.-Y. Kim, "Compact dual-wideband bandstop filter using a stub-enclosed stepped-impedance resonator," *AEU Int. J. Electron. Commun.*, vol. 70, no. 2, pp. 198–203, Feb. 2016.
[12] H. K. Chiou and C. F. Tai, "Dual-band microstrip bandstop filter using dual-mode loop resonator," *Electron. Lett.*, vol. 45, no. 10, pp. 507–509, May 2009.
[13] W. J. Feng, W. Q. Che, S. Y. Shi, and Q. Xue, "Compact dual-wideband bandstop filters based on open-coupled lines and transversal signal-interaction concepts," *IET Microw., Antennas Propag.*, vol. 7, no. 2, pp. 92–97, Jan. 2013.
[14] W. Wang, M. Liao, Y. Wu, and Y. Liu, "Small-size high-selectivity bandstop filter with coupled-line stubs for dual-band applications," *Electron. Lett.*, vol. 50, no. 4, pp. 286–288, Feb. 2014.
[15] C. Zhang, J.-P. Geng, R.-H. Jin, X.-L. Liang, and L. Liu, "Dual-wideband bandstop filter using stepped impedance coupled-lines," *Microw. Opt. Technol. Lett.*, vol. 57, no. 10, pp. 2304–2306, Oct. 2015.
[16] R. Dhakal and N.-Y. Kim, "A compact symmetric microstrip filter based on a rectangular meandered-line stepped impedance resonator with a triple-band bandstop response," *Sci. World J.*, vol. 2013, pp. 1–7, Jan. 2013.
[17] X. Min and H. Zhang, "Compact triple-band bandstop filter using folded, symmetric stepped-impedance resonators," *AEU Int. J. Electron. Commun.*, vol. 77, pp. 105–111, Jul. 2017.
[18] J. Ai, Y. H. Zhang, K. D. Xu, M. K. Shen, and W. T. Joines, "Miniaturized frequency controllable band-stop filter using coupled-line stub-loaded shorted SIR for tri-band application," *IEEE Microw. Wireless Compon. Lett.*, vol. 27, no. 7, pp. 627–629, Jul. 2017.
[19] S. Yang, Z. Xiao, and S. Budak, "Design of triband bandstop filters using a stub-loaded stepped-impedance resonator," *Prog. Electromagn. Res. Lett.*, vol. 90, pp. 69–75, 2020.
[20] S. Yang, Z. Xiao, and S. Budak, "Design of triband bandstop filter using an asymmetrical cross-shaped microstrip resonator," *Prog. Electromagn. Res. Lett.*, vol. 86, pp. 35–42, 2019.
[21] K. K. Adhikari and N. Y. Kim, "A miniaturized quad-band bandstop filter with high selectivity based on shunt-connected, T-shaped stub-loaded, stepped-impedance resonators," *Microw. Opt. Technol. Lett.*, vol. 57, no. 5, pp. 1129–1132, May 2015.
[22] R. Dhakal, S. Cho, B. Shrestha, and C. Seo, "Quad-band bandstop filter modeled by comprising quad-section stepped-impedance resonator," *Anal. Integr. Circuits Signal Process.*, vol. 98, no. 1, pp. 147–153, Jan. 2019.
[23] P. Wang, H. Yang, Z. Yu, X. Huang, and Y. Jin, "A compact quad-band bandstop filter using square spiral resonators based on folded stepped impedance resonator," in *Proc. 11th Int. Symp. Antennas, Propag. EM Theory (ISAPE)*, Oct. 2016, pp. 766–768.
[24] I. Hunter, *Theory and Design of Microwave Filters*, vol. 48. Edison, NJ, USA: IET, 2001.
[25] S. Khalid, W. P. Wen, and L. Y. Cheong, "Synthesis and design of four pole ultra-wide band (UWB) bandpass filter (BPF) employing multi-mode resonators (MMR)," in *IEEE MTT-S Int. Microw. Symp. Dig.*, Jun. 2012.

MUHAMMAD FAISAL was born in Pakistan, in 1985. He received the Bachelor of Science degree in telecommunication engineering from the National University of Computer and Emerging Sciences, Islamabad, Pakistan, and the Master of Science degree in electrical and electronic engineering from the University of Bradford, U.K. He is currently pursuing the Ph.D. degree in electrical engineering with the Department of Electrical Engineering, Riphah International University, Pakistan.

He is currently a Senior Lecturer with the Department of Electrical Engineering, Riphah International University. His current research interest includes designing of RF and microwave passive devices.

SOHAIL KHALID (Member, IEEE) received the B.Eng. (Hons.) degree from CIIT Islamabad, Pakistan, in 2008, the M.Sc. degree in wireless networks from the Queen Mary University of London, in 2009, and the Ph.D. degree from Universiti Teknologi PETRONAS, Malaysia, in 2014.

He is currently serving as an Associate Professor and the Head of Department of Electrical Engineering, Riphah International University, Islamabad, where he is teaching various undergraduate and postgraduate engineering courses. His research interests include synthesis and design of passive microwave devices, millimeter wave applications for biomedical engineering, and biomedical signal processing.

MUJEEB UR REHMAN received the bachelor's and M.S. (Hons.) degrees in electrical engineering from Riphah International University, Islamabad, Pakistan, where he is currently pursuing the Ph.D. degree in electrical engineering.

He is also working as a Lecturer with Riphah International University. His current research interest includes RF engineering and iris-based disease diagnosis.

MUHAMMAD ABDUL REHMAN received the bachelor's and M.Sc. degrees in computer sciences and telecom systems from Bahauddin Zakariya University, Multan, Pakistan, and the M.S. degree in electrical engineering from Riphah International University, Islamabad, Pakistan, where he is currently pursuing the Ph.D. degree in electrical engineering.

He is also working as a Demonstrator with Riphah International University. His current research interest includes RF and microwave passive devices.